Structural characterization of iron sulfide tribofilms formed on carbon and stainless steels

Makoto Miyajima (miyajima.qe3.makoto@jp.nipponsteel.com)
Nippon Steel Corporation https://orcid.org/0000-0002-9125-9063
Mitsuharu Yonemura
Nippon steel
Kazuyuki Kitamura
Nippon steel
Keishi Matsumoto
Nippon steel
Kazuyuki Yagi
Kyushu University: Kyushu Daigaku

Research Article

Keywords: polysulfide, sulfur-containing additives, stainless steel, tribofilm, scuffing

Posted Date: June 2nd, 2022

DOI: https://doi.org/10.21203/rs.3.rs-1672579/v1

Abstract

Extreme pressure (EP) additives are used to reduce friction and improve the wear resistance of lubricants that are used in engine and gear systems in vehicles and cold working process. Sulfur-containing EP additives react with the metal surface to form inorganic tribofilms, such as those containing iron sulfide, with a relatively low shearing strength that prevents scuffing. In this study, tribofilms formed under boundary lubrication via the reaction of a polysulfide additive on carbon steel (S45C) and stainless steel (SUS304) surfaces were investigated using four *ex situ* techniques, namely, X-ray photoelectron spectroscopy, Raman spectroscopy, X-ray diffraction analysis, and transmission electron microscopy, to understand the causes of scuffing in stainless steel. In the tests conducted with the SUS304 disc, the friction coefficient increased more slowly compared to that of the S45C disc and showed fluctuations. The tribofilm on the S45C disc comprised the outermost and inner layers of FeS_2 (pyrite) and FeS (troilite) structures, respectively. Conversely, the tribofilm on the SUS304 disc surface possessed an FeS_2 structure in both the outermost and inner layers. The tribofilm on the SUS304 disc exhibited poor crystallinity in the outermost layer and was thinner than that formed on the S45C disc. The formation of a weaker tribofilm on the SUS304 disc probably introduced instability of the friction coefficient and scuffing.

1. Introduction

Extreme pressure (EP) additives are widely used in many industries such as engine and gear systems for vehicles [1, 2] and cold working of metals [3]. EP additives such as molybdenum dithiocarbamate (MoDTC) [4] and zinc dialkyldithiophosphate (ZDDP) [5, 6] have been added to engine oil in recent years. MoDTC reduces friction by forming an MoS_2 tribofilm on the contact area [7–10] whereas ZDDP prevents wear by forming an amorphous tribofilm with multi-layered structures [5, 6, 11]. The role of metallic and non-metallic substrates in the tribochemical reaction of MoDTC [12–14] and ZDDP [15–17] has been the focus of recent studies.

Chlorine-containing EP additives are widely used in the cold working process of steel because they are relatively cost effective and exhibit high lubricity even for stainless steel with high corrosion resistance [3]. However, its use is restricted owing to environmental and public health hazards, such as carcinogenicity. Much effort has been made to develop chlorine-free lubricating oils. However, the use of chlorine-free additives is still limited in the cold reduction of metal working for two reasons. First, for high-alloy steels used in applications that require a high degree of corrosion resistance, such as the energy-related industry, chlorine-based additives are still utilized during cold working processes to prevent scuffing. Second, there is a concern that specific elements in additives may invade the steel and affect its mechanical properties if the heat treatment process is initiated with the retention of the lubricating oil during processing. Additionally, phosphorus-containing additives such as ZDDP cannot be used to cause embrittlement of steel. Sulfur-containing EP additives such as mono-, di-, and poly-sulfides, which are less toxic to the environment than chlorine-containing additives, are expected to be used as an alternative to chlorine-containing EP additives in the cold working of steel.

The structures of tribofilms, formed as a result of chemical reactions between steel and sulfur-containing EP additives, have been extensively investigated [3, 18–27]. Sulfur-containing EP additives react with the steel surface to form inorganic tribofilms, such as iron sulfide, with a relatively low shearing strength that prevents scuffing. The FeS crystal, which has a hexagonal crystal structure, exhibits a low-shear strength[28, 29]. Wheeler *et al*. [18] reported that FeS or FeS_2 tribofilms with $FeSO_4$ contaminants are formed with sulfur-containing EP additives. Lara *et al.* [19] reported that dimethyl disulfide thermally decomposes on iron surfaces via half-order kinetics to yield a film comprising only FeS at temperatures as low as 523 K. However, Miyajima *et al.* [22, 23] reported that polysulfide chemically reacts with carbon steel during the rubbing process to yield a film composed of FeS_2 and graphite structure. These results indicate that changes in the chemical composition of the tribofilms ultimately depend on the applied load, speed, temperature, and chemical structure of the EP additives used for the various types of tribo-testers. However, many studies have employed carbon steel for experimentation.

Few studies have reported the chemical reactions between stainless steel and sulfur-containing EP additives [3, 18, 21, 26]. The structures of the tribofilms formed from chlorine- and sulfur-containing EP additives on stainless steel were investigated using Auger electron spectroscopy (AES) and X-ray photoelectron spectroscopy (XPS) [3]. Matsumoto *et al.* [21] investigated tribofilms formed from polysulfide on carbon, stainless steel, other high alloys, Ni, and Cr using XPS. They reported that materials containing a large amount of Fe formed thick tribofilms. They also found that materials with films indicating a high hardness exhibited low friction. However, the reason why materials with a large amount of Fe form thick tribofilms is unclear. They did not investigate the chemical and crystal structures of the tribofilms over the entire thickness range because they only conducted XPS. To prevent scuffing and to replace chlorine-containing additives with sulfur-containing ones, a detailed investigation of the structure of the tribofilm on the steel type is necessary.

In this study, the structures of tribofilms formed from polysulfide on carbon steel and stainless steel were investigated using four *ex situ* techniques: XPS [7, 10, 16, 21, 30], Raman spectroscopy [8, 9, 12–14, 22, 23, 31–34], X-ray diffraction (XRD) analysis [12, 13, 35–40], and transmission electron microscopy (TEM) [7, 11, 14–16] to understand the causes of scuffing in stainless steel.

2. Experimental Methods

2.1. Tribotests

The tribometer used in this study was a ball-on-disc-type tester, as shown in Fig. 1. It creates a point contact between a stationary steel ball with a diameter of 6.35 mm, and a rotating steel disc with a diameter and thickness of 20 and 3 mm, respectively. The stationary ball was composed of high-carbon-bearing steel of JIS SUJ2 (1.0 C-1.45 Cr mass%), which is equivalent to AISI 52100. Table 1 lists the chemical compositions and properties of the disc materials. The rotating discs were ferrite and perlite structures of the carbon steel JIS S45C, which is equivalent to AISI 1045, and an austenitic stainless steel SUS304, which is equivalent to AISI 304. The Vickers hardness values of the discs were the same, that is,

200 HV at room temperature. The thermal conductivities of S45C and SUS304 were 45 and 16 W/mK, respectively, at room temperature. The discs were polished with 3 μm diamond paste before performing the tribotests, and their roughness after polishing was R_a = 32 nm. The tests were performed under lubricating conditions. In the tests, a load of 10 N was applied, which produced a maximum Hertzian contact pressure of 0.94 GPa. The sliding speed, temperature, and duration of the tribotests were 10 mm/s, 200°C, and 20 min, respectively. The lubricant used was undiluted polysulfide (di(tert-dodecyl)penta sulfide: $C_{12}H_{25}$-S_5-$C_{12}H_{25}$, 127 mm^2/s kinematic viscosity (40°C)) as the sulfur-containing EP additive. Figure 2 shows the thermogravimetry (TG) and differential thermal analysis (DTA) results of the polysulfide. The sample with a weight of 10 mg was heated in dry air at a speed of 10°C/min. Evaporation of the polysulfide caused a weight loss of about 10% at 200°C. The endothermic reaction occurred at 228°C due to the decomposition of polysulfide, and the exothermic reaction occurred at 269°C due to combustion. An extreme test conditions was required to form thick tribofilms for performing structural analysis. The test temperature was set to 200°C, which is the maximum temperature up to which polysulfide decomposition does not occur. In addition, the polysulfide was undiluted to increase its reactivity. After conducting the tribotests, the discs were rinsed with acetone in an ultrasonic bath for 2 min, and then analyzed using four *ex situ* techniques.

Table 1
Chemical compositions and properties of the disc materials (mass%)

Material	C	Si	Mn	Ni	Cr	Fe	Phase and Structure	Hardness (HV)	Thermal conductivity (W/mK)
S45C	0.45	0.23	0.83	0.01	0.12	98.3	Ferrite, perlite	200	45
SUS304	0.05	0.54	1.50	8	18	71.9	Austenite	200	16

2.2. Chemical structure analysis of the outermost layer

XPS and Raman spectroscopy were used to investigate the chemical structure of the outermost layer of the tribofilms after performing the tribotests. XPS was conducted to investigate the chemical composition of the surface at a depth of approximately 5 nm. It was conducted using a PHI QuanteraSXM spectrometer with a monochromatized Al Kα irradiation source with a spot size of 50–100 μm in diameter. The analyzer pass energy was 55.0 eV. Raman spectroscopy was conducted using an HR800 microspectrometer (HORIBA Jobin Yvon). The excitation laser used for Raman spectroscopy had a wavelength of 532 nm, which was produced by a diode-pumped solid-state laser. The Raman spectra were acquired using a 50× long-working distance objective lens with a numerical aperture of 0.50. This objective lens achieved a spatial resolution of 2 μm in diameter. The Raman spectra were obtained at room temperature in ambient air. The acquisition time for each Raman spectrum was 120 s.

2.3. Inner layer analysis

XRD analysis and TEM were performed to investigate the inner layers of the tribofilms. XRD analysis was performed using a Rigaku RINT-RAPID instrument with a Co target operated at 40 kV and 15 mA. X-rays were incident at an angle of 30° using a collimator with a diameter of 500 μm. An area with a diameter of 1,000 μm on the sliding surface was measured. The penetration depth of X-rays was approximately 3–6 μm. Cross-sectional TEM images of the tribofilms were obtained using a TEM with an acceleration voltage of 200 kV after extraction using a focused ion beam instrument. The electron diffraction pattern of the tribofilms was obtained. Point analysis of each material was performed at three points of the tribofilms using energy-dispersive X-ray spectroscopy (EDX).

3. Results

3.1. Tribotests

Figure 3 shows the variations in the friction coefficients during the tests for the S45C and SUS304 discs. Three tests were conducted under the same operating conditions for each disc. The friction coefficient exceeded 0.6 rapidly within 2 min after the beginning of the tests and then remained steady at approximately 0.55 in all tests for the S45C discs. In contrast, the friction coefficients of the SUS304 discs increased more slowly than those of the S45C discs and fluctuated during the three tests. The friction coefficient with the red line shown in Fig. 3 (b) increased gradually to 0.5, over 5 min after the beginning of the test. The final friction coefficient of the SUS304 discs was approximately 0.5–0.6, which is comparable to that of the S45C discs.

Figure 4 shows optical images of the wear scar on the balls and discs after completion of the tribotests shown in Fig. 3. The wear scars shown in Fig. 4 (a) and (b) correspond to the test for the S45C disc which yielded the friction coefficient plotted in red, as shown in Fig. 3(a). Both wear scars were approximately 700 μm wide. The wear scars shown in Fig. 4 (c) and (d) correspond to the test for the SUS304 disc which yielded the lowest friction coefficient plotted in red in Fig. 3(b). The wear scars shown in Fig. 4 (c) and (d) were approximately 500 and 600 μm wide, respectively. The wear scars shown in Fig. 4 (e) and (f) correspond to the test for the SUS304 disc resulting in the highest friction coefficient, indicated by the blue color in Fig. 3 (b), whose widths were approximately 480 and 800 μm, respectively. The wear scar of the SUJ2 ball depended on the counter disc. The wear scar on the ball surface with the S45C disc shown in Fig. 4 (b) appears to be the result of corrosion wear. Conversely, the wear scar on the ball surface with the SUS304 disc shown in Fig. 4 (d) appears to be caused by scuffing. The wear scar of the ball surface with the SUS304 disc shown in Fig. 4 (f) is larger and appears be more scuffed than the wear scar of the SUJ2 ball in Fig. 4 (d). When the discs in Fig. 4 (a), (c), and (e) were compared, the widths of wear scars of the SUS304 disc were observed to be narrower than those of the S45C discs. Therefore, we conclude that the SUS304 disc has a low narrower tribo-reaction film to be prone to scuff than the S45C disc.

3.2. XPS

XPS was performed to obtain information about the elements and chemical bonds on the surfaces. Table 2 and Fig. 5 show the XPS quantification and spectra of the outermost surfaces on the wear scars of the S45C and SUS304 discs after the tribotests, respectively. The S45C (blue line in Fig. 3 (a)) and SUS304 discs (green line in Fig. 3 (b)) were analyzed. The elements C, O, S, and Fe were detected on the wear scars of both the discs, as shown in Table 2. In addition, N, Cr, and Ni were detected only on the surface of the SUS304 disc. The atomic ratios of S/Fe in S45C and SUS304 were approximately 2.4 and 3.0, respectively. The tribofilm on the SUS304 disc had a higher S/Fe ratio than that on S45C. Figure 5 shows the XPS spectra of (a) O 1s, (b) Fe $2p_{3/2}$, and (c) S 2p acquired on the wear scars of S45C and SUS304 discs, along with (d) Cr $2p_{3/2}$, and (e) Ni $2p_{3/2}$ acquired on the wear scars of the SUS304 disc. The chemical structures of the peaks were identified by the handbook [41], as mentioned in previous studies [21]. Large C-O and/or C = O peaks at 532 eV were detected on the wear scars of both discs, while a small iron oxide peak at 530 eV was detected on that of the S45C disc in the O 1s region. The chemical bonds of C-O/C = O may originate from the decomposition of polysulfide and contamination. Large FeS_2 peaks at 707.2 eV and small iron oxide peaks at 711.0 eV were detected in the Fe $2p_{3/2}$ region for both discs. Large FeS_2 peaks at 164 and 162.5 eV and a broad iron sulfate peak at 168.8 eV were detected in the S 2p region for both discs. These peak positions of FeS_2 were slightly different in S45C and SUS304 discs due to the structural differences of FeS_2 tribofilms. The chemical bonds of the Cr_2O_3 peak at 576.5 eV and the Cr_2S_3 peak at 575 eV were scarcely detected in the Cr $2p_{3/2}$ region of the SUS304 disc. The chemical bond of the NiS_2 peak at 853.7 eV was scarcely detected in the Ni $2p_{3/2}$ region too. Comprehensively, the main structure of the outermost layer of the tribofilms comprised FeS_2 on the wear scars of the S45C and SUS304 discs.

Table 2
XPS quantification of the outermost surface on the wear scars of the S45C and SUS304 discs after tribotests (at.%)

	C 1s	O 1s	S 2p	N 1s	Fe $2p_{3/2}$	Cr $2p_{3/2}$	Ni $2p_{3/2}$
S45C	34	31.1	24.5	-	10.4	-	-
SUS304	44	22.9	22.9	0.8	7.7	1.5	0.3

3.3. Raman spectroscopy

Figure 6 shows the Raman spectra obtained (a) on the wear scar and (b) unworn surface of the S45C and SUS304 discs after the tribotests. In Fig. 6 (a), the S45C (red line in Fig. 3 (a)) and SUS304 (red line in Fig. 3 (b)) discs were analyzed. The peaks at 335, 365 and 416 cm^{-1} on the wear scar of S45C disc were identified as FeS_2 [22, 23, 27, 42, 43]. The sharp peaks at 335 and 365 cm^{-1} can be observed to be clearly separated. The peaks at 331 and 361 cm^{-1} detected from the wear scars of the SUS304 disc were also identified with FeS_2 as well as S45C disc. These peaks are broad and not clearly separated. Moreover, these peaks are seen to be shifted to lower wavenumbers compared to those for the S45C disc. The

broad peaks from 1,200 to 1,650 cm^{-1} on both the discs were identified as the D and G bands of the graphite structure. These peaks were generated from the decomposition of polysulfide during the formation of the FeS_2 tribofilm [22, 23, 27]. The small peaks at 660 cm^{-1} on both discs were identified with Fe_3O_4 [44]. In Fig. 6 (b), the broad peaks at 331 and 379 cm^{-1} identified as FeS_2 were detected on the unworn surface of the S45C disc. This FeS_2 is considered to have been formed by a thermal reaction, with reference to the TG-DTA results shown in Fig. 2. No peak was detected on the unworn surface of the SUS304 disc.

3.4. XRD analysis

Figure 7 shows the XRD patterns of the wear scars of the S45C (green line in Fig. 3 (a)) and SUS304 (blue line in Fig. 3 (b)) discs. The peaks of α-Fe and Fe_3C (cementite) for the S45C disc were derived from substrates with body-centered cubic (BCC) structures. The phases of γ and α'-Fe of SUS304 disc were derived from substrates with face-centered cubic (FCC) and deformation-induced martensite structures, respectively. Crystal grains of FeS_2 (pyrite) and FeS (troilite) were detected on the wear scars of the S45C disc. Contrarily, only crystal grains of FeS_2 (pyrite) were detected on the wear scars of the SUS304 disc. The FeS_2 tribofilm peaks detected at 66 and 73° on the S45C discs shifted toward smaller angles on the SUS304 discs.

3.5. TEM observation

Figure 8 shows cross-sectional TEM images of the tribofilms on the S45C (red line in Fig. 3 (a)) and SUS304 (red line in Fig. 3 (b)) discs. The thickness profile of the tribofilm on the S45C disc was in the 300 to 600 nm range. The tribofilm on the SUS304 disc had a thickness of approximately 300 nm, which is half the thickness of the tribofilm on the S45C disc. A white layer, considered to be an oxide film, was formed between the substrate and tribofilm in the S45C disc, whereas no oxide film was observed between the substrate and tribofilm on the SUS304 disc. Figure 9 shows the cross-sectional TEM images and electron diffraction patterns of the tribofilms on the S45C and SUS304 discs. Electron diffraction patterns were obtained from the region of a diameter of approximately 200 nm in the cross-sectional tribofilm layers. The tribofilm on the S45C disc exhibited a uniform diffraction pattern, identified with an FeS structure, whereas that on the SUS304 disc surface exhibited a dot-like pattern, identified with an FeS_2 structure. These results show that the FeS tribofilm on the S45C disc had fine crystal grains, whereas the FeS_2 tribofilm on the SUS304 disc possessed coarse crystal grains.

Figure 10 shows the cross-sectional TEM image and EDX spectra of the tribofilms on the S45C disc. Oxygen was not detected at the point 01 away from the interface between the substrate and tribofilm, whereas it was detected at the point 02 and 03 near the substrate. Figure 11 shows the cross-sectional TEM image and EDX spectra of the tribofilm on SUS304. Oxygen was detected at all points in Fig. 11, but there was less oxygen at points 01 and 02 away from the substrate and more at the interface (point 03) with the substrate. These results indicate that an oxide film exists at the interface between the substrate

and tribofilm on both the discs. Particularly, Cr and O peaks at point 03 were stronger than at point 01 and 02 in Fig. 11. This indicates that the Cr_2O_3 film exists at the interface between the substrate and tribofilm on SUS304.

4. Discussion

4.1. Differences between the tribofilm structures on the S45C and SUS304 discs

The structure of the tribofilms was thoroughly investigated using four *ex situ* techniques. Table 3 shows the results obtained for the tribofilm structures on the S45C and SUS304 discs using these techniques. The penetration depth of the laser in Raman spectroscopy is expressed as 1/2α, where α is the absorption coefficient of the substance. In the case of FeS_2, $\alpha = 1.5 \times 10^5\ cm^{-1}$ for light with a wavelength of approximately 500 nm, as shown in Fig. S7 in Wu *et al*. [45]. In this study, the penetration depth was approximately 33 nm. The outermost layer of the tribofilms on both the S45C and SUS304 discs were identified to be FeS_2 using XPS and Raman spectroscopy. However, the FeS_2 tribofilm on the SUS304 disc exhibited poorer crystallinity than that on the S45C disc as indicated by the broad Raman peaks of the tribofilm on the SUS304 disc than those on the S45C disc. This is observed because Cr and Ni were mixed in the tribofilm on the SUS304 disc, as shown in Table 2.

According to the results of the XRD analysis shown in Fig. 7, both FeS and FeS_2 peaks were detected for the S45C disc, whereas only FeS_2 peaks were detected for the SUS304 surface. Conversely, the diffraction patterns in the tribofilms analyzed using TEM indicated that the tribofilm on the S45C disc was identified with fine FeS crystal grains, whereas that on the SUS304 disc was identified with coarse FeS_2 crystal grains, as shown in Fig. 9. In summary, the tribofilm created on the S45C disc comprised an outermost layer of FeS_2 and an inner layer of FeS, whereas the tribofilm created on the SUS304 surface consisted of only FeS_2 from the outermost to the inner layer.

The TEM observations indicated that the thickness of the tribofilm on the S45C disc was twice that of the SUS304 disc, as shown in Fig. 8. The austenitic stainless steel of SUS304, which has a lower thermal conductivity, tends to raise the temperature of the sliding surface compared to the S45C disc. Although this is expected to improve the reactivity of the tribofilm on SUS304 than on S45C, the experimental results of the present study displayed the opposite trend. We believe that the formation of the oxide film affected the formation process of the tribofilm. A Cr_2O_3 passive film is generally formed on the surface of SUS304 [46]. This Cr_2O_3 passive film prevented the thermal reaction with polysulfide, as shown in Fig. 6 (b). Therefore, at the beginning of the tribotest, this Cr_2O_3 passive film on the surface suppressed the formation of tribofilm. In addition, the formation of a Cr_2O_3 passive film at the interface of the tribofilm and SUS304 substrate was considered to suppress the growth of the tribofilm.

Figure 12 shows a schematic of the mechanism that causes the difference in the formation of tribofilms between S45C and SUS304. An iron oxide film existed at the interface between the substrate and the tribofilm on the S45C disc, but it did not cover the entire interface evenly, as observed in Fig. 8 (a). At the atomic level, substitution between the Fe atoms in the iron oxide and the substrate occurred easily because they were the same atom. Therefore, the inner layer of the tribofilm on the S45C disc was composed of FeS owing to the diffusion of Fe from the substrate, while the outermost layer of the tribofilm was composed of FeS_2 because of the S-rich environment in contact with the polysulfide (Fig. 12 (a)).

In contrast, SUS304 formed a dense Cr_2O_3 passive film on its surface in the atmosphere and water, which prevented the diffusion of Fe atoms from the SUS304 substrate to the surface (Fig. 12 (b)). This suppressed the tribochemical reaction between Fe and the polysulfide. The Cr_2O_3 passive film was not directly observed at the interface between the SUS304 substrate and the FeS_2 tribofilm, as shown in Fig. 8 (b), because it was very thin (approximately 2–3 nm) [46]. However, the existence of passive Cr_2O_3 film was suggested from the EDX point analysis in Fig. 11 (d). Since the tribofilm undergoes repeated formation and destruction during the wear process, a continuous supply of Fe from the substrate is necessary to form an iron sulfide tribofilm. The Cr_2O_3 passive film is considered to suppress Fe diffusion to make the tribofilm thinner. The tribofilm on the SUS304 disc was composed of only the FeS_2 structure from the inside to the outermost layer of the film because the diffusion of Fe was suppressed by the Cr_2O_3 passive film.

Table 3
Results of the formation of tribofilm structures on the S45C and SUS304 discs using the four *ex situ* techniques

Technique	Observed layer	S45C	SUS304
XPS	Outermost	FeS_2	FeS_2
Raman spectroscopy	Outermost	FeS_2	FeS_2 (Poor crystallinity)
XRD	Inner and outermost	FeS, FeS_2	FeS_2
TEM/Diffraction	Inner	FeS (Fine crystal)	FeS_2 (Coarse crystal)

4.2. Reasons for SUS304 being prone to scuffing

Various hypotheses, such as differences in the structure and thermal conductivity of the surface, and formation of chemical reaction films on the surface, can be used to explain as to why the SUS304 surface is prone to scuffing. Under dry conditions, the lower thermal conductivity of SUS304 can explain why the SUS304 surface is more likely to scuff than the S45C surface. This is because materials with low thermal conductivity raise the temperature of the sliding surfaces. In a lubricating oil environment, the difference in thermal conductivity alone cannot explain the difference in scuffing because the formation

of chemical reaction films on the surface is expected to be more important to prevent wear and scuffing. We believe that the difficulty in the formation of a tribofilm on the SUS304 disc is one of the most important reasons for its surface being prone to scuff. The S45C surface is considered to prevent scuffing because of the formation of a thick tribofilm, whereas the SUS304 surface produces a thinner tribofilm with a poorer structure owing to the existence of the Cr_2O_3 layer, as discussed earlier. The difference in the tribofilm structure between the S45C and SUS304 discs should also be considered. The FeS (troilite) crystal found in the tribofilm on the S45C disc possesses a hexagonal close-packed (HCP) structure whose lattice constants are a = 0.597 nm and c = 1.174 nm [28]. It can easily slip along the close-packed direction in the close-packed plane. In contrast, FeS_2 (pyrite), which comprises the tribofilm on the SUS304 disc, has a cubic structure. The FeS tribofilm fares better than the FeS_2 tribofilm in terms of scuffing. Ueda *et al*. reported that the ZDDP tribofilm was nanocrystallized from an amorphous state by friction, and its durability was improved [11]. Since the tribofilm on S45C possesses better crystallinity in the outermost layer and fine crystal grains in the inner layer, it may be more durable than the tribofilm on SUS304.

As discussed above, the presence of the Cr_2O_3 passive film on the stainless steel surface can be presumed to cause scuffing because of the suppression of tribofilm formation, which reduces the tribofilm thickness and changes it to a structure that is less likely to be sheared. To prevent the scuffing of stainless steel, it is necessary to develop an additive that directly reacts with the Cr_2O_3 film to decompose it to form a tribofilm. Chlorine-containing EP additives that have been used so far are probably effective in reacting with the Cr_2O_3 film via the chlorine anion and forming a chlorine-containing tribofilm with a low shear resistance. A lubricating oil component that possesses both these properties is required to replace sulfur.

5. Conclusions

In this study, tribofilms from polysulfide additive formed under boundary conditions were investigated. Tribotests, which create a contact area between a stationary steel ball and rotating steel disc, were conducted. Two types of steel, namely, carbon steel (S45C) and austenitic stainless steel (SUS304) were used to investigate the influence of the surface material on the structure of the tribofilm. Several surface analysis techniques, namely, XPS, Raman spectroscopy, XRD analysis, and TEM were employed to investigate the structure of the tribofilm. The conclusions are summarized as follows:

(1) The wear scar of the ball surface after the tests with the S45C disc seemed to indicate corrosive wear. Scuffing was observed for the SUS304 disc.

(2) After the test with the S45C disc, the tribofilm created on the disc had a mixed structure comprising of an outermost layer of FeS_2 crystal grains and an inner layer of FeS crystal grains.

(3) The tribofilm formed on the SUS304 disc comprised FeS_2 crystal grains throughout its layers. The outermost layer exhibited poor crystallinity.

(4) The Cr_2O_3 passive film created on the SUS304 disc probably prevented the diffusion of Fe atoms from the bulk material to the surface. Consequently, the Cr_2O_3 passive film suppressed the tribochemical reaction, causing instability of friction and scuffing.

(5) The tribofilm with FeS crystal grains formed on the S45C disc, which had an HCP structure and fine crystal grains, can probably contribute to low friction and prevent scuffing.

Declarations

Acknowledgments

The authors would like to thank Mr. Syoichiro Inoue, Ms. Kaoru Fujita, and Mr. Nobuhito Maeda for their assistance with the experimental work. They would also like to express thanks to Ms. Akiko Ito for conducting XPS and Ms. Yuri Higaki for TEM.

References

1. Kato M, Matsuzaki Y, Yagi K, Sugimura J. Influence of crystal grain structure of steel surface on formation of chemical reaction film derived from engine oil additives. Tribology International. 2020;151. https://doi.org/10.1016/j.triboint.2020.106458
2. Espejo C, Wang C, Thiébaut B, Charrin C, Neville A, Morina A. The role of MoDTC tribochemistry in engine tribology performance. A Raman microscopy investigation. Tribology International. 2020;150. https://doi.org/10.1016/j.triboint.2020.106366
3. Petrushina IM, Christensen E, Bergqvist RS, Møller PB, Bjerrum NJ, Høj J, et al. On the chemical nature of boundary lubrication of stainless steel by chlorine- and sulfur-containing EP-additives. Wear. 2000;246:98–105. https://doi.org/10.1016/s0043-1648(00)00503-2
4. Sakurai T, Okabe H, Isoyama H. The synthesis of di-μ-thio-dithio-bis (dialkyldithiocarbamates) dimolybdenum (V) and their effects on boundary lubrication. Bulletin of the Japan Petroleum Institute. 1971;13:243–9. https://doi.org/10.1627/jpi1959.13.243
5. Spikes H. The history and mechanisms of ZDDP. Tribology Letters. 2004;17:469–89. https://doi.org/10.1023/B:TRIL.0000044495.26882.b5
6. Parsaeian P, Ghanbarzadeh A, Van Eijk MCP, Nedelcu I, Neville A, Morina A. A new insight into the interfacial mechanisms of the tribofilm formed by zinc dialkyl dithiophosphate. Applied Surface Science. 2017;403:472–86. https://doi.org/10.1016/j.apsusc.2017.01.178
7. Komaba M, Kondo S, Suzuki A, Kurihara K, Mori S. The effect of temperature on lubrication property with MoDTC-containning lubricant. Tribology Online. 2018;13:275–81. https://doi.org/10.2474/trol.13.275
8. Khaemba DN, Neville A, Morina A. A methodology for Raman characterisation of MoDTC tribofilms and its application in investigating the influence of surface chemistry on friction performance of MoDTC lubricants. Tribology Letters. 2015;59. https://doi.org/10.1007/s11249-015-0566-6

9. Khaemba DN, Neville A, Morina A. New insights on the decomposition mechanism of Molybdenum DialkyldiThioCarbamate (MoDTC): a Raman spectroscopic study. RSC Advances. 2016;6:38637–46. https://doi.org/10.1039/c6ra00652c
10. Komaba M, Kondo S, Suzuki A, Kurihara K, Mori S. Kinetic study on lubricity of MoDTC as a friction modifier. Tribology Online. 2019;14:220–5. https://doi.org/10.2474/trol.14.220
11. Ueda M, Kadiric A, Spikes H. On the crystallinity and durability of ZDDP tribofilm. Tribology Letters. 2019;67. https://doi.org/10.1007/s11249-019-1236-x
12. Tanabe T, Ito T, Oyama Y. Structure and optical properties of 2D layered MoS_2 crystals implemented with novel friction induced crystal growth. AIP ADVANCES. 2018;8:035122. https://doi.org/10.1063/1.5022247
13. Tanabe T, Ito T, Chen M, Oyama Y. Effect of the surface texture at the interface on the friction induced crystal growth of 2D layered MoS_2. Journal of Nanosciences: Current Research. 2018;3. https://doi.org/10.4172/2572-0813.10000127
14. Tanabe T, Osaki J, Miyajima M, Kitamura K, Oyama Y. Raman and TEM characterization of 2D layered MoS_2 crystals grown on non-metal surfaces by friction-induced synthesis. Applied Surface Science. 2021;561:150016. https://doi.org/10.1016/j.apsusc.2021.150016
15. Ueda M, Kadiric A, Spikes H. ZDDP tribofilm formation on non-ferrous surfaces. Tribology Online. 2020;15:318–31. https://doi.org/10.2474/trol.15.318
16. Ueda M, Kadiric A, Spikes H. Influence of steel surface composition on ZDDP tribofilm growth using ion implantation. Tribology Letters. 2021;69. https://doi.org/10.1007/s11249-021-01436-8
17. Pagkalis K, Spikes H, Jelita Rydel J, Ingram M, Kadiric A. The influence of steel composition on the formation and effectiveness of anti-wear films in tribological contacts. Tribology Letters. 2021;69. https://doi.org/10.1007/s11249-021-01438-6
18. Wheeler DR. X-ray photoelectron spectroscopic study of surface chemistry of dibenzyl disulfide on steel under mild and severe wear conditions. Wear. 1978;47:243–54. https://doi.org/10.1016/0043-1648(78)90155-2
19. Lara J, Blunt T, Kotvis P, Riga A, Tysoe WT. Surface chemistry and extreme-pressure lubricant properties of dimethyl disulfide. J Phys Chem B. 1998;102:1703–9. https://doi.org/10.1021/jp980238y
20. Najman MN, Kasrai M, Bancroft GM. X-ray absorption spectroscopy and atomic force microscopy of films generated from organosulfur exreme-pressure (EP) oil additives. Tribology Letters. 2003;14:225–35. https://doi.org/10.1023/A:1022650516272
21. Matsumoto K, Miyajima M, Kitamura K. Characterization of boundary lubrication film formed on Fe-Cr-Ni alloy by means of XPS —Influence of Cr and Ni contents on formation of boundary lubrication film—. Tribologist(Japanese). 2014;59:636–47.
22. Miyajima M, Kitamura K, Matsumoto K. Characterization of tribofilm with the remaining lubricating oil by Raman spectroscopy. Tribology Online. 2015;10:225–31. https://doi.org/10.2474/trol.10.225

23. Miyajima M, Kitamura K, Matsumoto K. In situ Raman tribometry for the formation and removal behavior of FeS_2 tribofilm in the scuffing process. Tribology Online. 2016;11:382–8. https://doi.org/10.2474/trol.11.382
24. Monasse B, Montmitonnet P. DFT-modeling of the reaction of a polysulfur extreme-pressure lubricant additive on iron surface. Int J Mater Form. 2008:1251–4. https://doi.org/10.1007/s12289-008-0169-y
25. Li J, Ma H, Ren T, Zhao Y, Zheng L, Ma C, et al. The tribological chemistry of polysulfides in mineral oil and synthetic diester. Applied Surface Science. 2008;254:7232–6. https://doi.org/10.1016/j.apsusc.2008.05.298
26. Mori S, Imaizumi Y. Adsorption of model compounds of lubricant on nascent surfaces of mild and stainless steels under dynamic conditions. Tribology Transactions. 1988;31:449–53. https://doi.org/10.1080/10402008808981847
27. Dairene U, Steven SJ, Ann ONE, Ronald JK. Raman characterization of anti-wear films formed from fresh and aged engine oils. SAE Technical paper. 2006:01–1099. https://doi.org/10.4271/2006-01-1099.
28. Wang H-D, Xu B-S, Liu J-J, Zhuang D-M. Characterization and tribological properties of plasma sprayed FeS solid lubrication coatings. Materials Characterization. 2005;55:43–9. https://doi.org/10.1016/j.matchar.2005.02.007
29. Wang H-D, Zhuang D-M, Wang K-L, Liu J-J. Anti-scuffing properties of ion sulfide layers on three hard steels. Wear. 2002;253:1207–13. https://doi.org/10.1016/s0043-1648(02)00231-4
30. Rossi A, Eglin M, Piras FM, Matsumoto K, Spencer ND. Surface analytical studies of surface-additive interactions, by means of in situ and combinatorial approaches. Wear. 2004;256:578–84. https://doi.org/10.1016/j.wear.2003.10.001
31. Matsumoto K, Sagara M, Miyajima M, Kitamura K, Amaya H. Study of oil country tubular goods casing and liner wear mechanism on corrosion-resistant alloys. SPE Drilling & Completion. 2018;33:41–9. https://doi.org/10.2118/187946-PA
32. Miyajima M, Kitamura K, Matsumoto K, Yagi K. In situ temperature measurements of sliding surface by Raman spectroscopy. Tribology Letters. 2020;68. https://doi.org/10.1007/s11249-020-01356-z
33. Okubo H, Sasaki S. In situ Raman observation of structural transformation of diamond-like carbon films lubricated with MoDTC solution: Mechanism of wear acceleration of DLC films lubricated with MoDTC solution. Tribology International. 2017;113:399–410. https://doi.org/10.1016/j.triboint.2016.10.009
34. Yagi K, Vergne P, Nakahara T. In situ pressure measurements in dimpled elastohydrodynamic sliding contacts by Raman microspectroscopy. Tribology International. 2009;42:724–30. https://doi.org/10.1016/j.triboint.2008.10.005
35. Kajita S, Yagi K, Izumi T, Koyamachi J, Tohyama M, Saito K, et al. In situ X-ray diffraction study of phase tansformation of steel in scuffing process. Tribology Letters. 2015;57. https://doi.org/10.1007/s11249-014-0443-8

36. Yagi K, Kajita S, Izumi T, Koyamachi J, Tohyama M, Saito K, et al. Simultaneous synchrotron X-ray diffraction, near-infrared, and visible in situ observation of scuffing process of steel in sliding contact. Tribology Letters. 2016;61. https://doi.org/10.1007/s11249-015-0636-9
37. Izumi T, Yagi K, Koyamachi J, Saito K, Sanda S, Yamaguchi S, et al. Surface deteriorations during scuffing process of steel and analysis of their contribution to wear using in situ synchrotron X-ray diffraction and optical observations. Tribology Letters. 2018;66. https://doi.org/10.1007/s11249-018-1062-6
38. Yagi K, Izumi T, Koyamachi J, Sanda S, Yamaguchi S, Satio K, et al. In situ observation of crystal grain orientation during scuffing process of steel surface using synchrotron X-ray diffraction. Tribology Letters. 2020;68. https://doi.org/10.1007/s11249-020-01357-y
39. Bataev IA, Lazurenko DV, Bataev AA, Burov VG, Ivanov IV, Emurlaev KI, et al. A novel operando approach to analyze the structural evolution of metallic materials during friction with application of synchrotron radiation. Acta Materialia. 2020;196:355–69. https://doi.org/10.1016/j.actamat.2020.06.049
40. Emurlaev KI, Bataev IA, Lazurenko DV, Burov VG, Ivanov IV, Emurlaeva YY. Deformation-induced martensite transformation in AISI 321 stainless steel under dry sliding friction. Materials Today: Proceedings. 2020;25:424–7. https://doi.org/10.1016/j.matpr.2019.12.140
41. Moulder JF, Stickle WF, Sobol PE, Bomben KD. Handbook of X-ray photoelectron spectroscopy. Perkin-Elmer Corporation. 1992.
42. Vogt H, Chattopadhyay T, Stolz HJ. Complete first-order Raman spectra of the pyrite structure compounds FeS_2, MnS_2 and SiP_2. J Phys Chem Solids. 1983;44:869–73. https://doi.org/10.1016/0022-3697(83)90124-5
43. Turcotte SB, Benner RE, Riley AM, Li J, Wadsworth ME, Bodily D. Application of Raman spectroscopy to metal-sulfide surface analysis. Applied optics. 1993;32:935–8. https://doi.org/10.1364/AO.32.000935
44. Peikertová P, Vaculík M, Filip P, Kukutschová J. Raman microspectroscopy as a tool for characterization of brake wear debris. Proceedings of Nanocon, Brno, Czech Republic. 2012;10:23–5.
45. Wu L, Dzade NY, Gao L, Scanlon DO, Öztürk Z, Hollingsworth N, et al. Enhanced photoresponse of FeS_2 films: The role of marcasite-pyrite phase junctions. Advanced Materials. 2016;28:9602–7. https://doi.org/10.1002/adma.201602222
46. Sugimoto K, Matsuda S. Passive and transpassive films on Fe-Cr alloys in acid and neutral solutions, Mater. Sci. Eng. 1980;42:181–9. https://doi.org/10.1016/0025-5416(80)90027-0

Figures

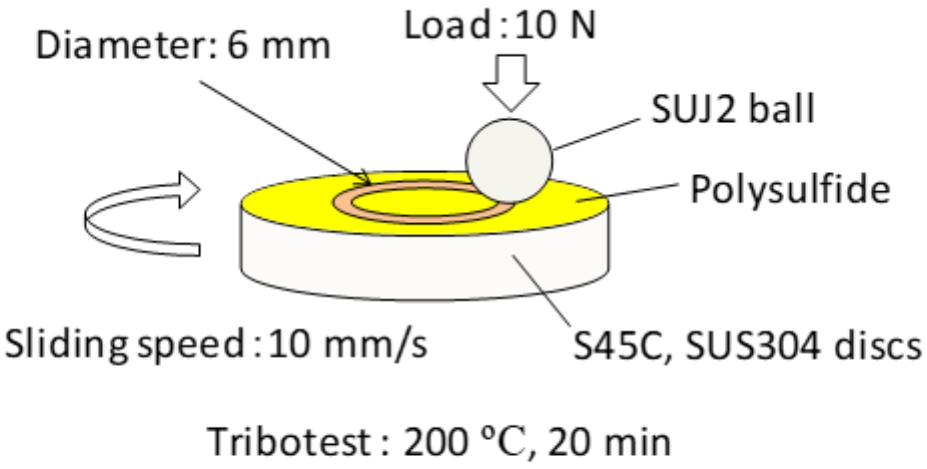

Fig. 1

Figure 1

Schematic of the ball-on-disc type tester

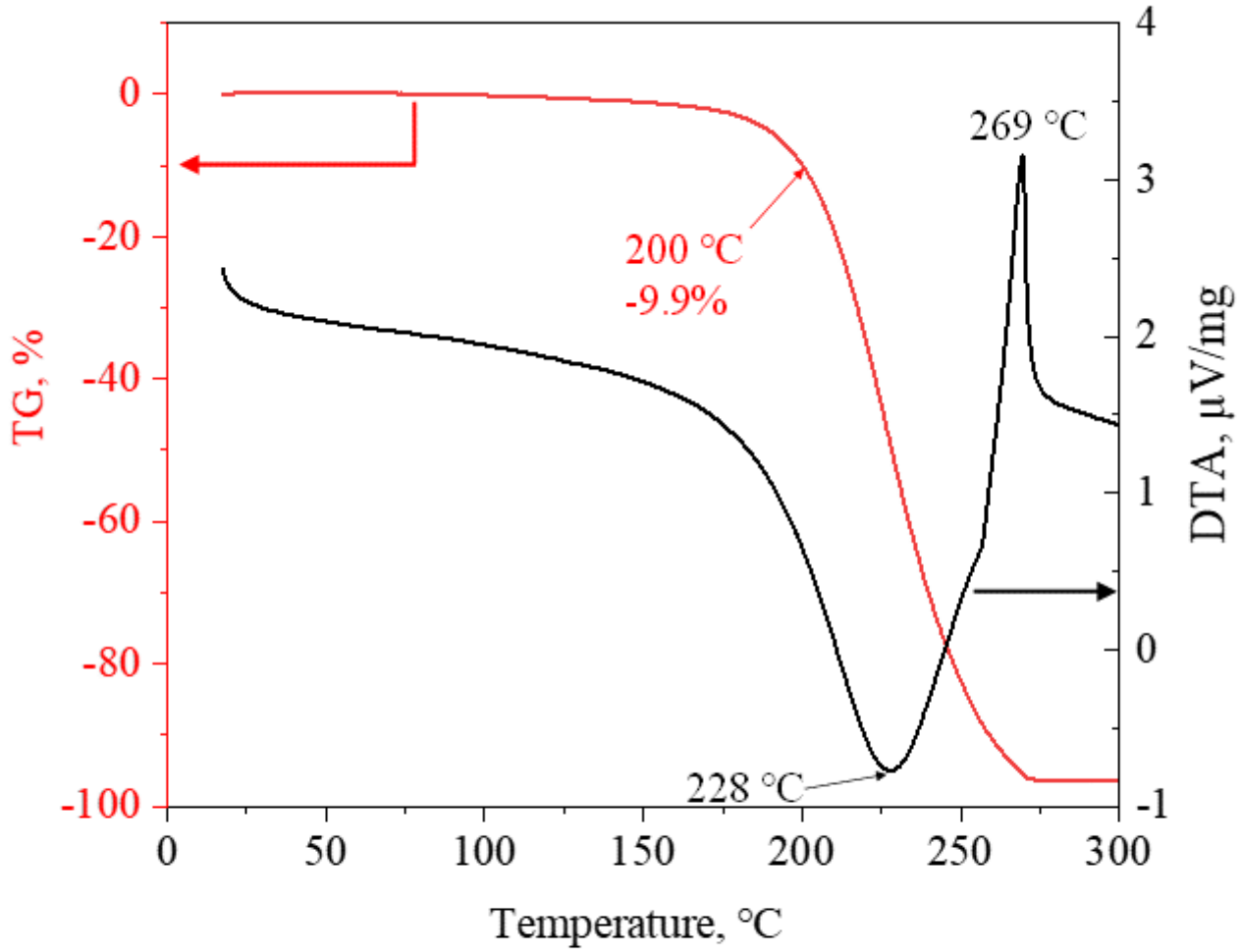

Fig. 2

Figure 2

TG-DTA profiles of the polysulfide

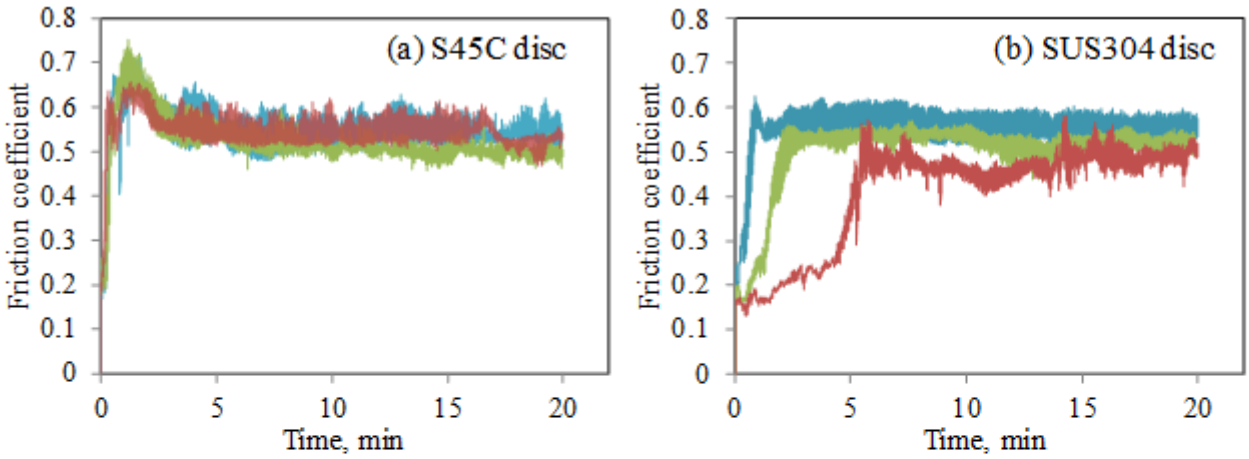

Fig. 3

Figure 3

Three test results of the friction coefficient behavior for the (a) S45C and (b) SUS304 discs

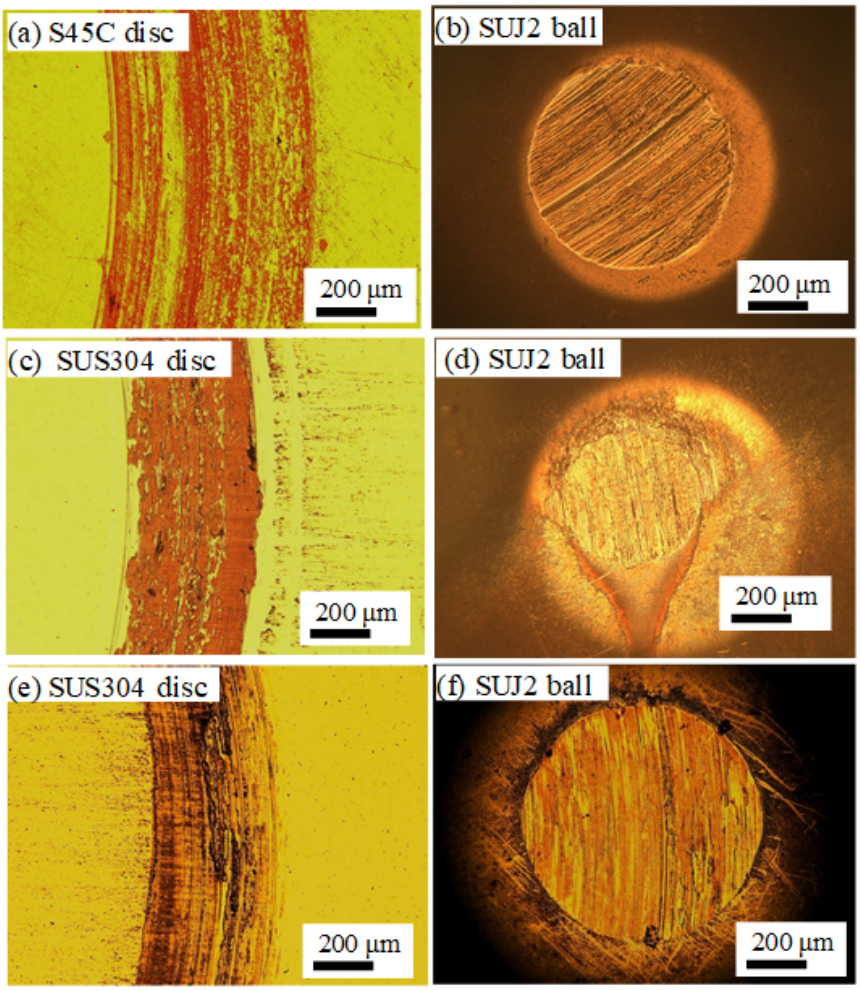

Fig. 4

Figure 4

Optical images of the discs and balls showing wear scars generated after the tribotests. Wear scars for the (a) S45C disc and (b) SUJ2 ball corresponding to the red line in Fig. 3 (a), (c) SUS304 disc and (d) SUJ2 ball corresponding to the red line with the lowest friction coefficient in Fig. 3 (b), and (e) SUS304 disc and (f) SUJ2 ball were obtained from the blue line with the highest friction coefficient, represented in blue, in Fig. 3 (b).

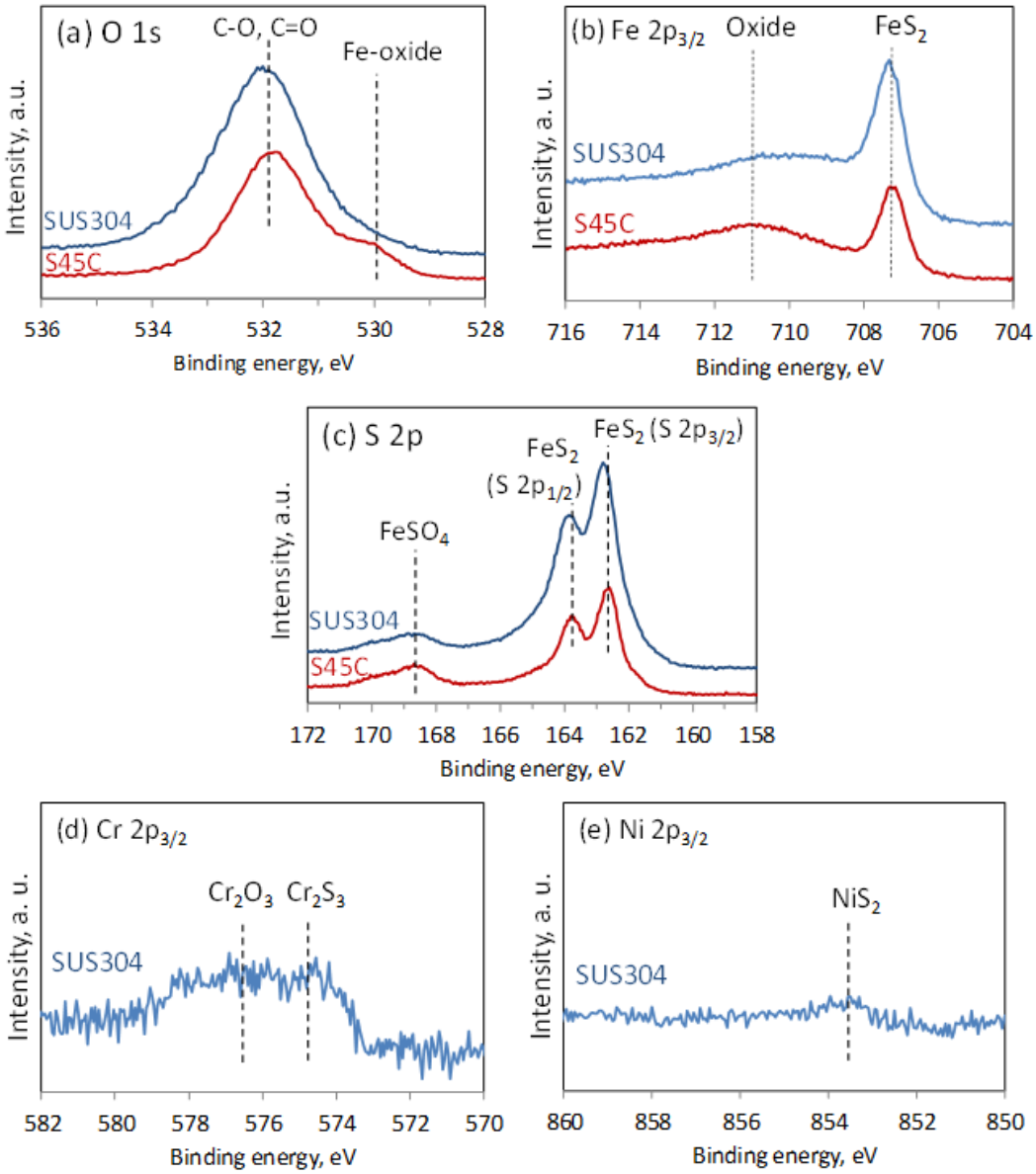

Fig. 5

Figure 5

XPS spectra obtained from the wear scars. (a) O 1s, (b) Fe $2p_{3/2}$ and (c) S 2p of the S45C and SUS304 discs, (d) Cr $2p_{3/2}$, and (e) Ni $2p_{3/2}$ of the SUS304 disc

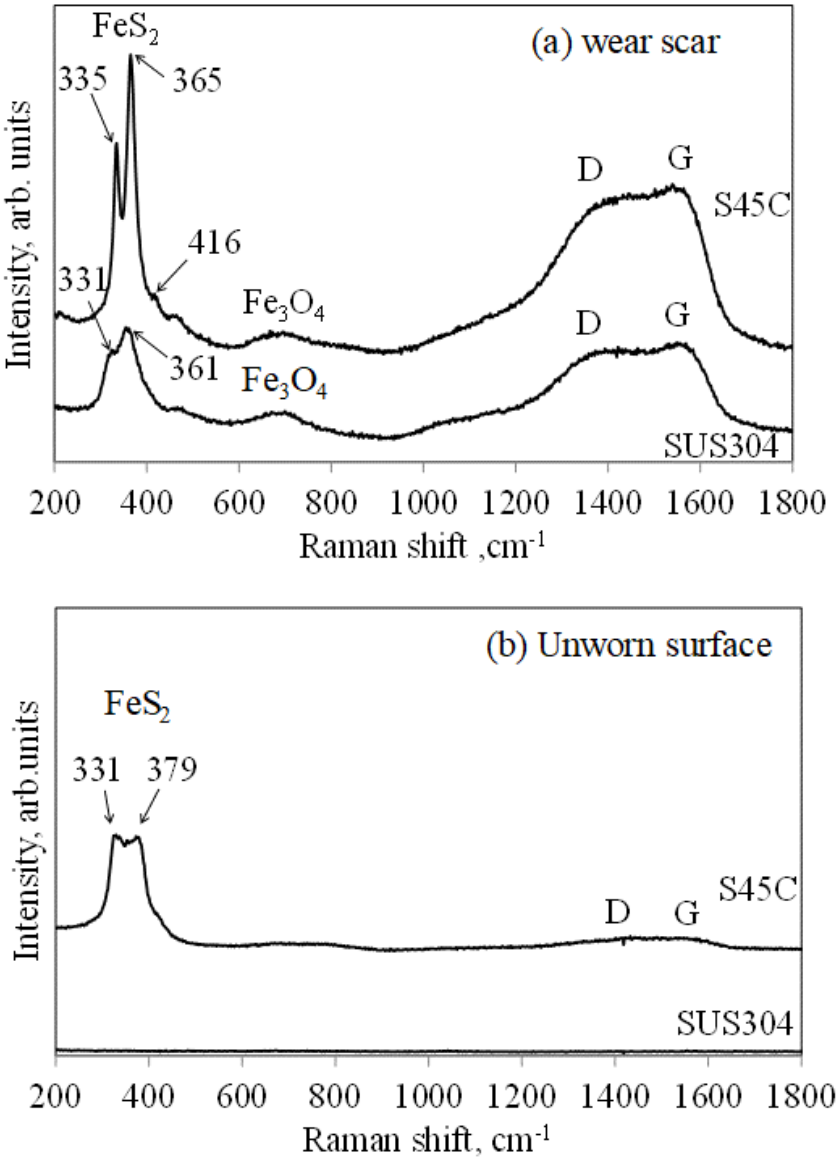

Fig. 6

Figure 6

Raman spectra of the S45C and SUS304 discs (a) on the wear scar and (b) unworn surface

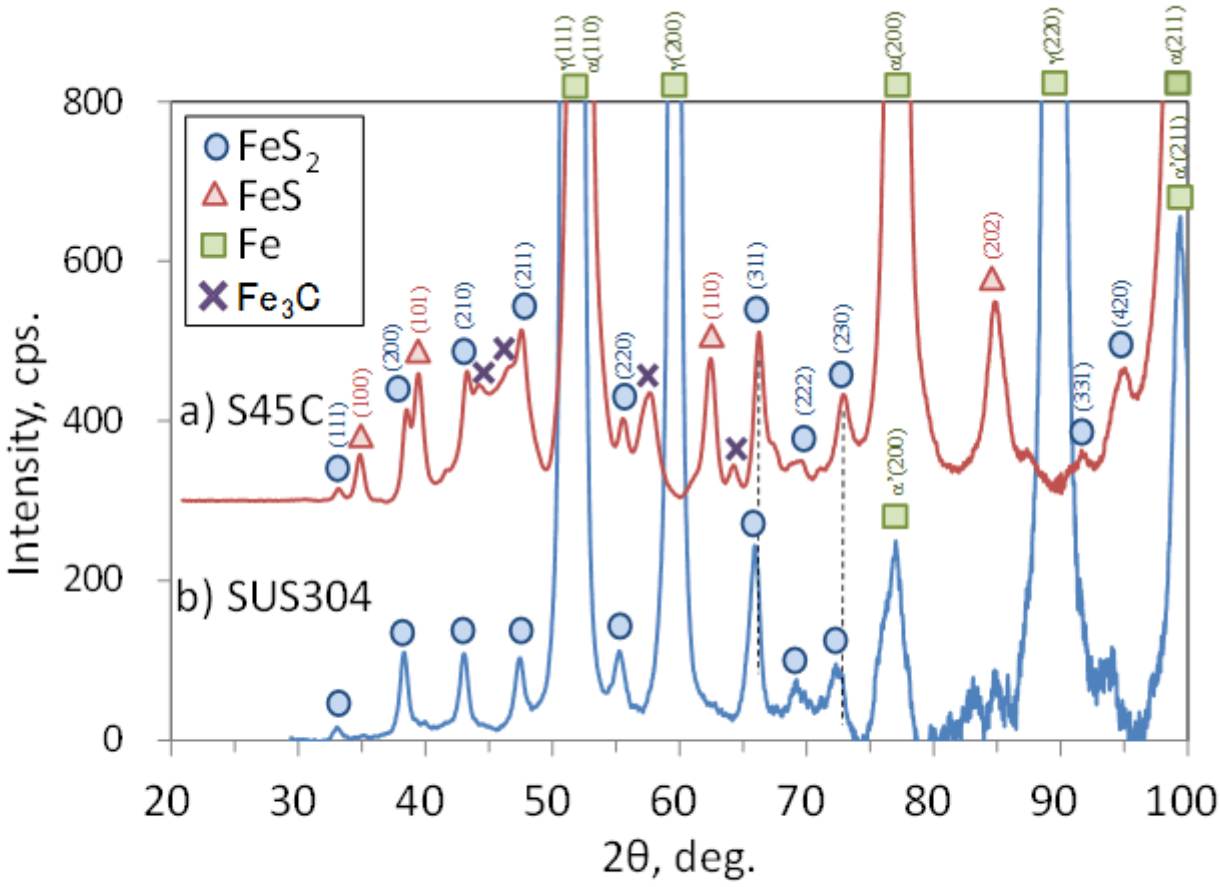

Fig. 7

Figure 7

XRD patterns of the wear scars of the a) S45C and b) SUS304 discs

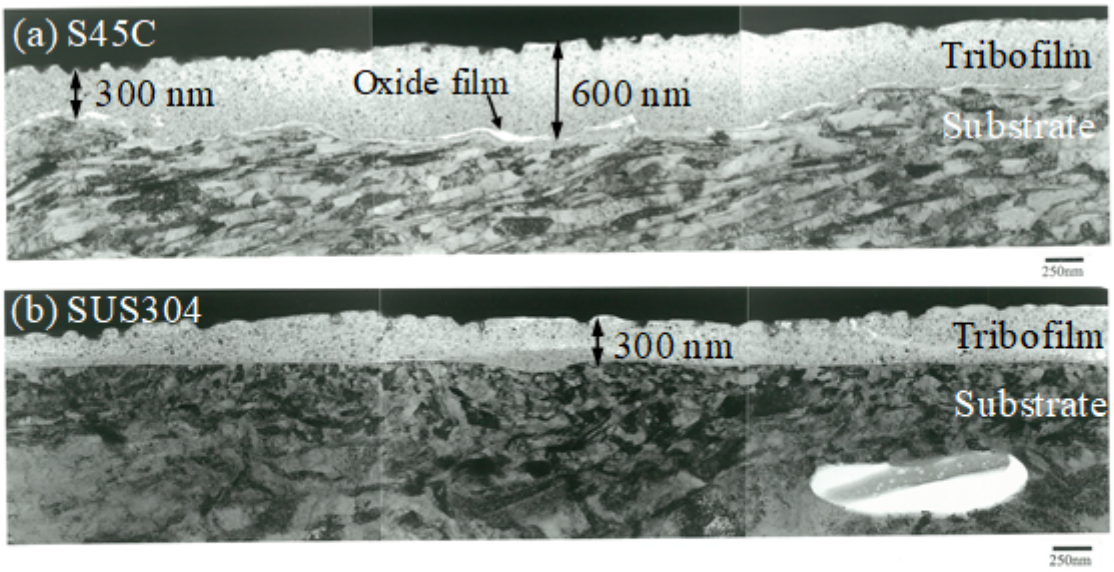

Fig. 8

Figure 8

Cross-sectional TEM images of tribofilms on the (a) S45C and (b) SUS304 discs

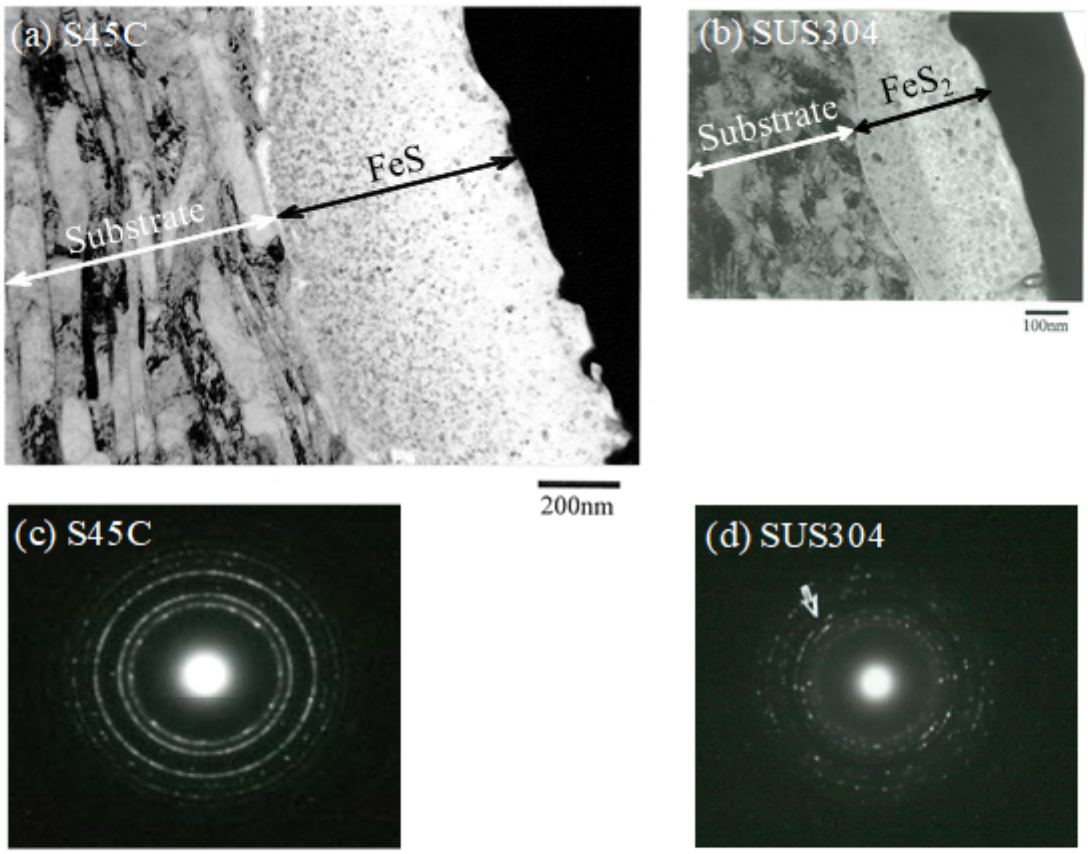

Fig. 9

Figure 9

Cross-sectional TEM images of the tribofilms on the (a) S45C and (b) SUS304 discs, and electron diffraction patterns of the tribofilms on the (c) S45C and (d) SUS304 discs

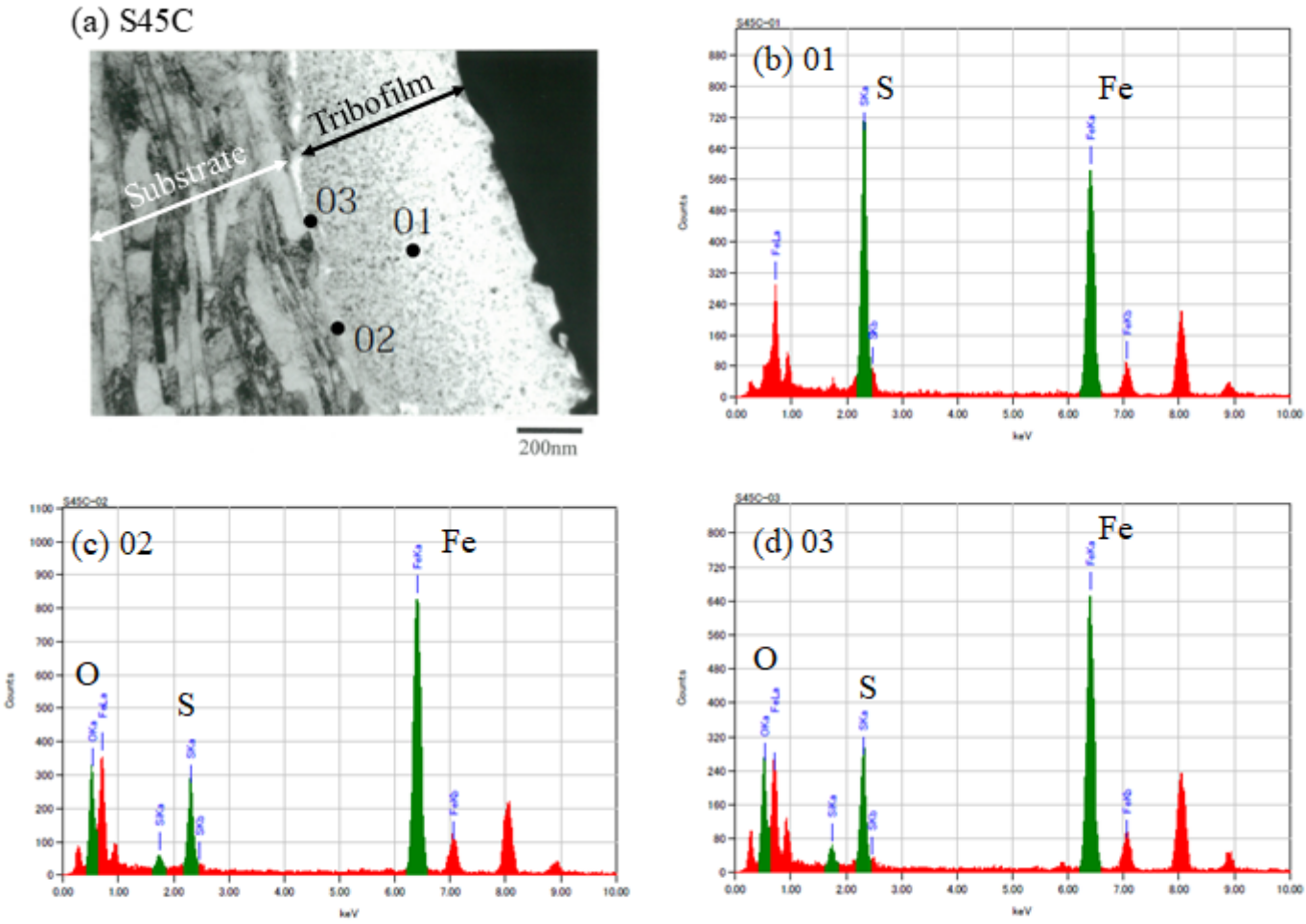

Fig. 10

Figure 10

(a) Cross-sectional TEM image of the S45C disk and the (b)–(d) EDX spectra

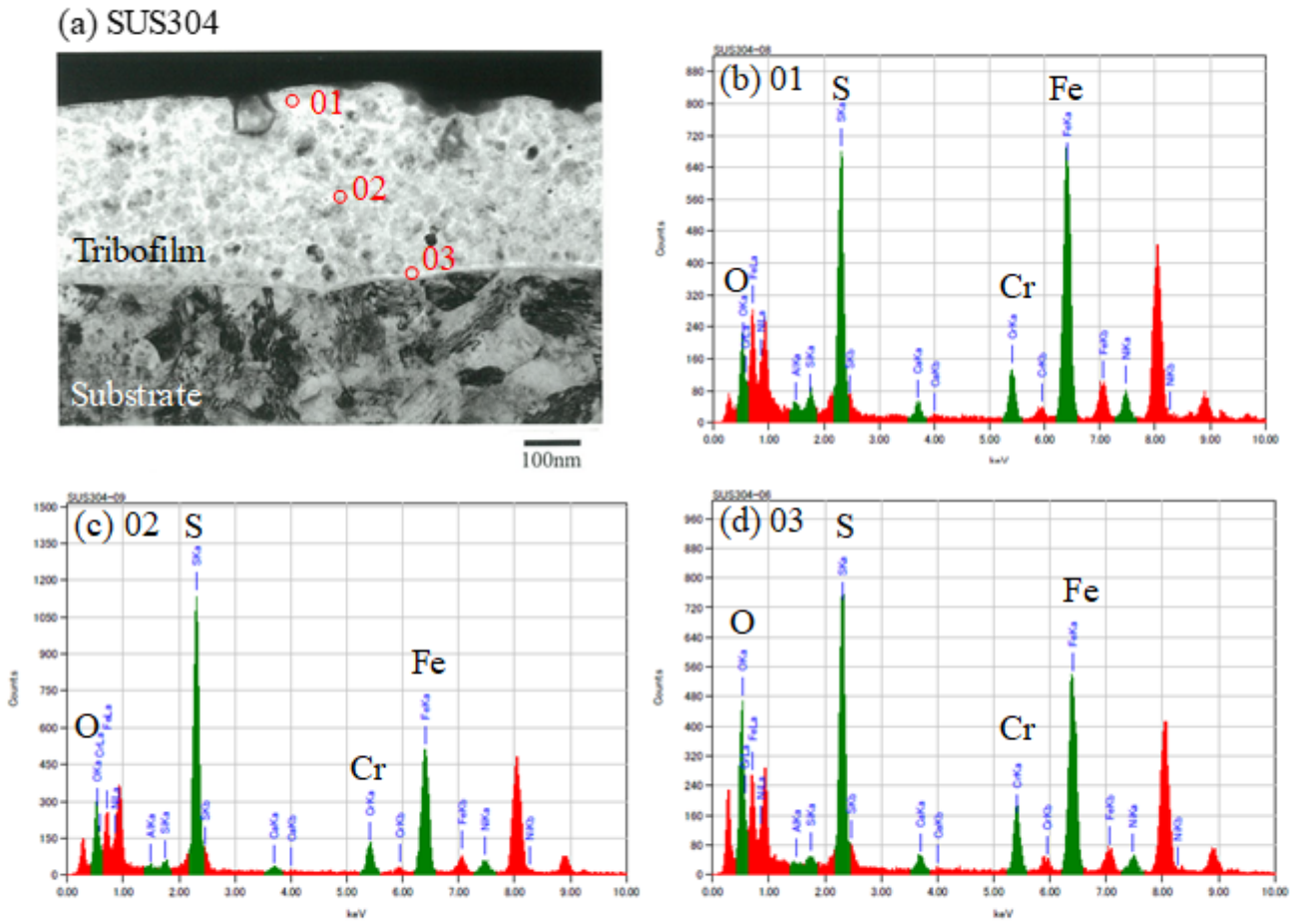

Fig. 11

Figure 11

(a) Cross-sectional TEM image of the SUS304 disk and the (b)–(d) EDX spectra

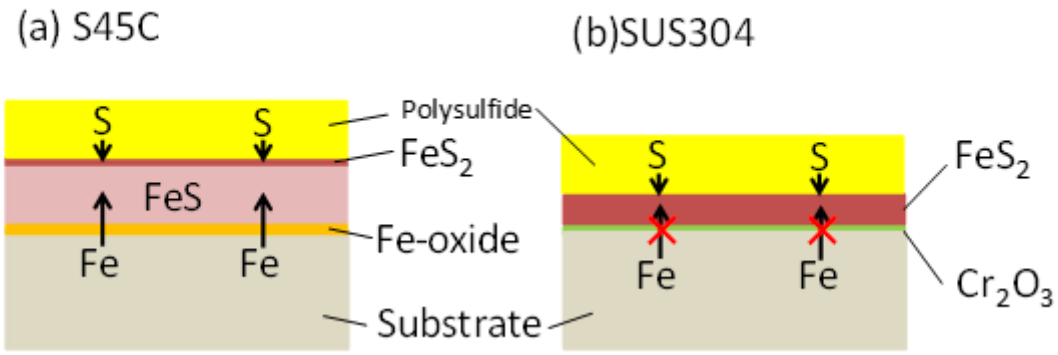

Fig. 12

Figure 12

Schematic of the mechanism of tribofilm formation on the (a) S45C and (b) SUS304 discs

Supplementary Files

This is a list of supplementary files associated with this preprint. Click to download.

- Graphicalabstract.pptx